Frontiers in Health Informatics
ISSN-Online: 2676-7104
www.healthinformaticsjournal.com
2024; Vol-13: Issue 8
Open Access

Comprehensive DFT Exploration of the Electronic Structure, Aromaticity, and Non-Covalent Interaction Landscape of Mavacamten

[1]D. Jebixson Immanuel and [2]J. Winfred Jebaraj*
[1]Research Scholar, Reg No: 21211272031008, Department of Chemistry,
St. John's College, Palayamkottai,
[2]Assistant Professor, Department of Chemistry,
St. John's College, Palayamkottai,
Affiliated to Manonmaniam Sundaranar University, Abishekapatti, Tirunelveli - 627002,
Tamil Nadu, India
Corresponding author: E-mail: winfred.chem@stjohnscollege.edu.in

Cite this paper as: D. Jebixson Immanuel and J. Winfred Jebaraj (2024). Comprehensive DFT Exploration of the Electronic Structure, Aromaticity, and Non-Covalent Interaction Landscape of Mavacamten. Frontiers in Health Informatics, Vol. 13, No.8, 7553-7565

Abstract
In this study, the molecular architecture and electronic properties of mavacamten—a selective cardiac myosin inhibitor used in the treatment of obstructive hypertrophic cardiomyopathy—were examined through a detailed density functional theory (DFT) investigation. Geometry optimization and electronic-structure calculations were performed using the B3LYP functional with the 6-311G(d,p) basis set. Mulliken charge analysis identified electron-rich and electron-deficient regions that govern the molecule's reactivity, while non-covalent interaction (NCI) mapping revealed the presence of steric congestion, van der Waals contacts, and weak hydrogen-bond features. Simulated scanning tunneling microscopy (STM) images provided insight into the spatial distribution of the local density of states, highlighting enhanced electronic activity around heteroatom sites. Aromaticity indices—including FLU, PDI, HOMA, BIRD, and PLR—confirmed a highly delocalized and structurally stable aromatic core. Further investigation of Laplacian electron density and Mayer bond orders clarified the balance between strongly conjugated carbon–carbon bonds and weak peripheral interactions. The Core–Valence Bifurcation (CVB) index indicated the predominance of weak hydrogen-bond interactions within the structure. Collectively, these computational findings deliver a comprehensive depiction of mavacamten's electronic landscape and bonding characteristics, providing a theoretical foundation for future structural modifications and mechanistic studies.

Keywords:
Mavacamten; DFT; Non-covalent interactions; sMayer bond order; Laplacian electron density; CVB index

1.Introduction

Mavacamten (marketed as **Camzyos**) is an innovative cardiovascular drug developed specifically for the treatment of **obstructive hypertrophic cardiomyopathy (HCM)**, a condition in which the heart muscle—particularly the left ventricle—becomes abnormally thick and excessively contractile. This excessive contraction obstructs the left ventricular outflow tract (LVOT), making it difficult for the heart to pump blood efficiently and ultimately

causing symptoms such as chest pain, shortness of breath, fatigue, and exercise intolerance [1, 2].

Traditional HCM therapies, including β-blockers, non-dihydropyridine calcium-channel blockers, and disopyramide, mainly focus on **symptomatic relief**, such as lowering heart rate or reducing overall workload on the heart. However, these approaches do not directly address the **underlying molecular abnormality** in HCM, which is the hypercontractile behavior of cardiac sarcomeres—the fundamental contractile units inside cardiac muscle cells [1]. Mavacamten represents a breakthrough because it acts precisely at the level of the **sarcomere**, treating the root cause rather than only its consequences.

At the molecular level, mavacamten works as a **selective, reversible inhibitor of cardiac myosin ATPase**, the enzyme responsible for powering the interaction between myosin and actin filaments. By binding to myosin, mavacamten promotes a special structural state known as the **super-relaxed state (SRX)**, in which fewer myosin heads are available to interact with actin. This reduces the number of active cross-bridges formed during cardiac contraction, thereby lowering the excessive force generation characteristic of HCM [2, 3]. As a result, the heart muscle relaxes more effectively during diastole, while LVOT obstruction decreases significantly, improving blood flow and reducing symptoms [3].

Clinical studies in adults with symptomatic obstructive HCM (NYHA class II–III) have shown that mavacamten can **decrease LVOT gradients, improve exercise capacity**, and enhance overall **quality of life**. In several major trials, patients treated with mavacamten demonstrated noticeable improvement in functional class and cardiac structure, making it one of the most promising disease-modifying therapies for HCM [4].

Pharmacokinetically, mavacamten displays high oral bioavailability and undergoes metabolism primarily through the **CYP2C19** pathway and secondarily via **CYP3A4**, which means certain genetic variations or drug interactions (such as inhibitors/inducers of these enzymes) can influence its plasma levels [1]. Because excessive reduction of cardiac contractility can potentially lower the left ventricular ejection fraction (LVEF), the drug requires **careful dose titration** and **regular echocardiographic monitoring** throughout treatment [1, 4].

The U.S. FDA approved mavacamten for adults with symptomatic obstructive HCM, marking a significant milestone in cardiovascular therapeutics. Instead of relying on invasive invasive procedures such as septal myectomy or alcohol septal ablation, many patients now have access to a **non-surgical, mechanism-based therapy** that directly targets sarcomeric dysfunction. With its precision-medicine approach, mavacamten has transformed the treatment paradigm for HCM and has opened new pathways for designing targeted therapies for other cardiac diseases linked to sarcomeric abnormalities [3, 5]. For such a molecule, no DFT approach is not yet done, therefore this molecule was subjected for further theoretical research.

2.Computational Methods

The quantum-chemical investigation of mavacamten was performed using density functional theory (DFT), employing Becke's three-parameter hybrid exchange functional in combination with the Lee–Yang–Parr (LYP) correlation functional (B3LYP) [6, 7]. All calculations were executed in the Gaussian 16W software suite [7, 8], which provides a reliable platform for geometry optimization and electronic structure analysis. For this study, the standard 6-311G(d,p) basis set was selected, as it offers a balanced level of accuracy by incorporating

polarization functions that enhance the description of molecular orbitals and electron distribution.

To visualize the optimized molecular structure and examine various molecular properties, GaussView 06 [9] was employed. This graphical interface facilitates the inspection of geometries, frontier molecular orbitals, vibration modes, and related quantum-chemical features. Further in-depth analyses were carried out using the Multiwfn 3.8 program [10], a versatile wavefunction analysis tool. Multiwfn 3.8 enabled the generation of surface projection maps and evaluation of non-covalent interactions, which provide valuable insights into weak molecular forces. Additionally, it was used to simulate scanning tunneling microscopy (STM) images, assess aromaticity indices, calculate Core–Valence Bifurcation (CVB) parameters, determine Mayer bond orders, and analyze Laplacian electron density distributions. Together, these computational tools offer a comprehensive understanding of the electronic structure, bonding features, and physicochemical characteristics of mavacamten. VMD 1.9 tool was used to view the outcomes of Multiwfn 3.8 results.

3.Results and discussion

3.1 Structural analysis

Mavacamten is a small molecule consisting of 39 atoms and 146 electrons and is a singlet, neutral in nature. A cardiac myosin inhibitor whose structure is built around a substituted **pyrimidinone** scaffold that imparts both rigidity and planarity to the molecule. A 2D and optimized 3D illustration of mavacamten is presented in Figure 1. The core ring system is connected to a **carbamate moiety**, which contributes to its hydrogen-bonding capability and overall polarity. The presence of **aromatic substituents** enhances π-electron distribution, supporting intermolecular interactions that influence binding affinity toward the myosin ATPase site. Several **functional groups**, including carbonyl, amide, and heterocyclic nitrogen atoms, contribute to electron delocalization and play significant roles in stabilizing the molecule's conformational states. The balance of hydrophobic and polar regions within the structure helps maintain optimal molecular flexibility for target engagement while supporting its pharmacokinetic characteristics. Overall, mavacamten's structural framework is designed to allow selective modulation of cardiac myosin function through well-oriented functional groups and a semi-rigid core that facilitates efficient receptor binding.

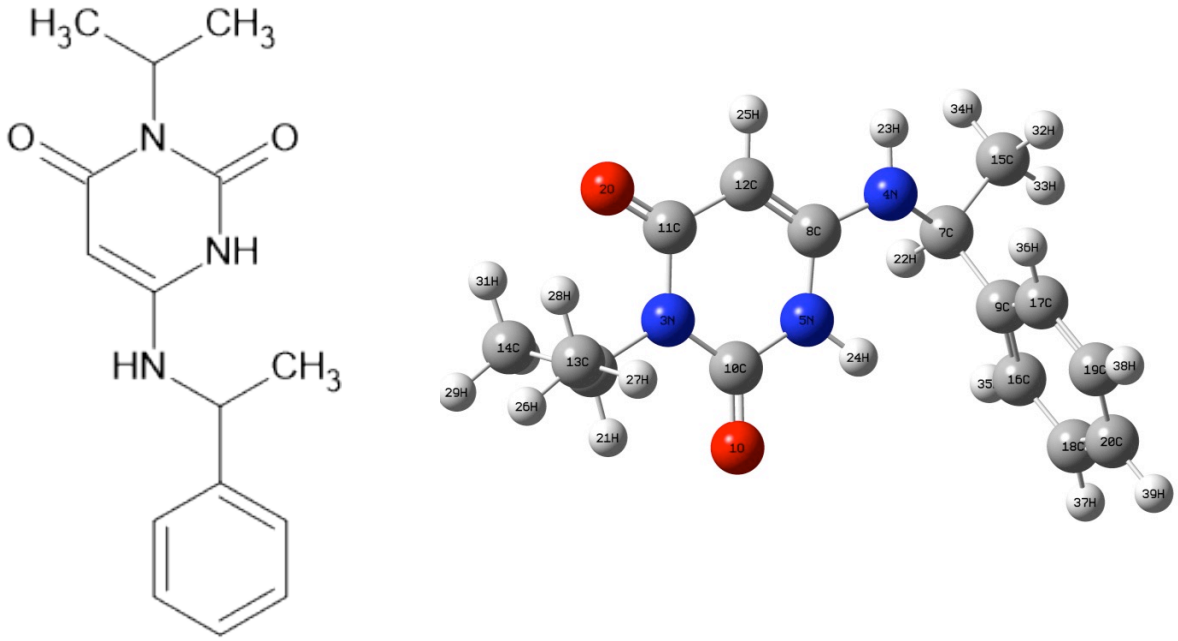

Figure 1: 2D and optimized 3D representation of mavacamten

3.2 Mullikan charge analysis

The Mulliken atomic charges of the target molecule were computed using the same level of theory and basis set, and the numerical values are summarized in Table 1. As shown in Table 1, the two oxygen atoms labeled 1O and 2O display nearly identical electronic characteristics, reflected by their Mulliken charge values of –0.5346 a.u. and –0.5343 a.u., respectively. The close similarity in these values indicates comparable electronic environments and suggests that both atoms may participate in similar chemical interactions or reactivity patterns. The carbon atom identified as 11C carries the highest positive charge in the molecule, with a value of +0.7346 a.u., indicating a strongly electron-deficient site. Conversely, the nitrogen atom labeled 3N exhibits the most negative charge, at –0.5447 a.u., signifying a region of pronounced electron density, and the graphical representation of Mullikan charge is depicted in Figure 2. These charge extremes highlight potential reactive centers within the molecule, which could be targeted for selective chemical modifications or considered important in molecular recognition processes.

Consistent with general chemical expectations, all hydrogen atoms exhibit positive Mulliken charges, reflecting their inherent electropositive nature. This trend is fully supported by the calculated charge values and corresponds well with observations in related molecular systems. Overall, the Mulliken charge distribution offers valuable insights into the electronic architecture of the molecule, enabling the identification of reactive hotspots that may be leveraged in future functionalization strategies or pharmacophore design.

Table 1: Mullikan charge of mavacamten

Atom	Charge (a.u)	Atom	Charge (a.u)	Atom	Charge (a.u)
1O	-0.5346	14C	-0.0268	27H	-0.0163
2O	-0.5343	15C	0.0020	28H	0.0385
3N	-0.5447	16C	-0.0265	29H	-0.0266

4N	-0.2008	17C	0.0077	30H	-0.0169
5N	-0.2267	18C	0.0297	31H	0.0391
6C	0.3659	19C	0.0212	32H	0.0080
7C	0.2637	20C	0.0129	33H	0.0079
8C	0.5475	21H	0.0162	34H	-0.0220
9C	-0.0693	22H	-0.0866	35H	0.0384
10C	0.7047	23H	0.1483	36H	0.0613
11C	0.7346	24H	0.2611	37H	0.0320
12C	-0.4989	25H	0.0569	38H	0.0297
13C	-0.0271	26H	-0.0257	39H	0.0347

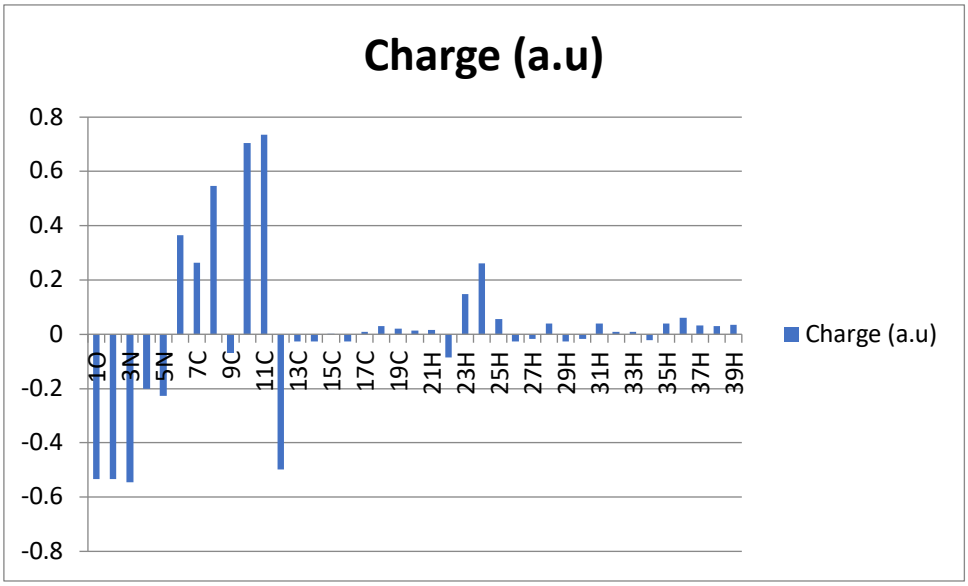

Figure 2: Mullikan charge graphical representation of mavacamten

3.3.Non covalent interactions

Relevant information on a molecule's non-covalent interactions can be found in the NCI analysis [11]. Johnson et al.'s noncovalent interactions (NCI) technique uses the reduced density gradient (s) to evaluate the molecular bonding and nonbonding interaction areas [12, 13]. It is described by,

$$RDG(r) = \frac{1}{2(3\pi^2)^{\frac{1}{3}}} \frac{|\nabla\rho(r)|}{\rho(r)^{\frac{4}{3}}} \quad (1)$$

The interactions were represented graphically in real space using the noncovalent interaction (NCI) technique. The hydrogen bond in the system under investigation was a little weaker. Figure 3 displays the RGD points plotted against electron density multiplied by the sign of the second eigenvalue (sign $(\lambda_2)\rho$) and the NCI plot. The map demonstrated high repulsion (steric repulsion), weak interaction (van der Waals attraction), and strong attraction (H-bonding).

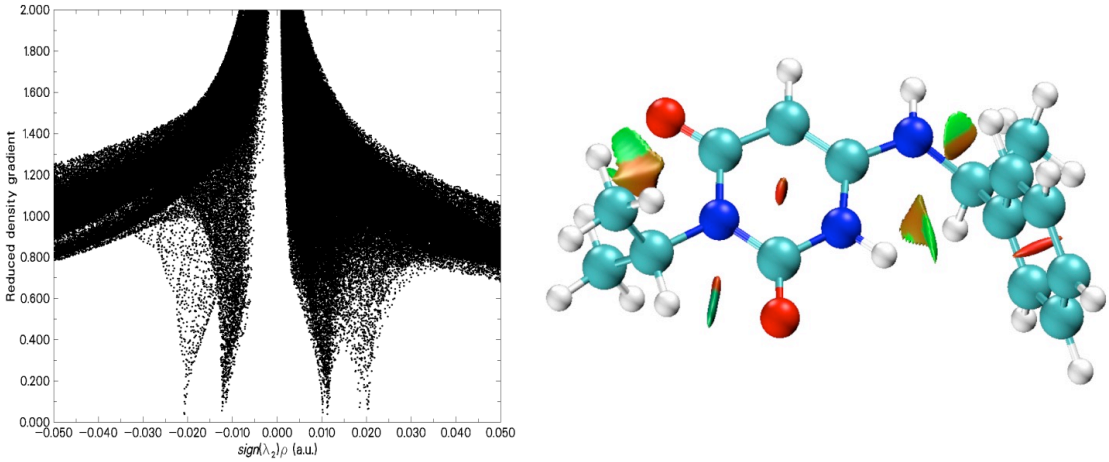

Figure 3: The non covalent interaction of mavacamten

The λ_2 sign is used to differentiate between bonded ($\lambda_2 < 0$) and non-bonded ($\lambda_2 > 0$) interactions [14]. In this instance, the function and λ_2 sign of the RDG scatter graph range from -0.050 to +0.050 a.u. The impact of steric repulsion [15] in the ring is caused by the peaks above +0.020 a.u. The spikes that appear in the $\lambda_2 = 0$ area indicate the van der Waals (vdW) forces (dipole-dipole interactions and London forces) [16]. Electrostatic interactions such as hydrogen and halogen bonds are represented by the spikes in the $\lambda_2 > 0$ and $\lambda_2 < 0$ regions. From Figure 3, it is clear that the steric factor is clearly identified as a red isosurface within the benzene ring. The hydrogen bond between -C-O...H-C is depicted as blue, while the van der Waals forces are represented as greenish brown iso-surfaces.

3.4.Scanning tunneling microscopy

Scanning tunneling microscopy is a highly sensitive technique used to visualize spatial variations in the tunneling current that arise at the junction between a sharp metallic tip and a conductive molecular surface [17]. In the present study, a simulated STM image for the title molecule is generated and analysed using Multiwfn 3.8, and the resulting map is shown in Figure 4. The calculated local density of states (LDOS) for mavacamten is found to be 0.5768 a.u. at an applied bias of V = –3.5 V and a tip–surface distance of Z = 0.5 Å. In this simulation, brighter white regions represent higher LDOS values, corresponding to stronger tunneling current (I), and according to the Tersoff–Hamann model, the tunneling current is directly proportional to the LDOS. The STM map clearly reveals that the tunneling signal is most intense around the heteroatoms—particularly oxygen and nitrogen—as well as certain carbon and ring-bound nitrogen atoms.

In addition to visualizing electron density, STM-based LDOS analysis provides valuable insight into the electronic structure of mavacamten that is relevant to its molecular behaviour and interaction profile. Mapping the spatial distribution of electrons helps identify regions with high electronic activity that may participate in noncovalent interactions such as hydrogen bonding, dipolar interactions, and π–π contacts, all of which are central to mavacamten's binding mechanism with cardiac myosin. The STM images also complement frontier molecular orbital analysis by revealing how the electronic cloud is distributed across the core bicyclic framework and peripheral functional groups, thereby offering a clearer picture of electronic delocalization and local reactivity. This integrated electronic mapping improves understanding of how specific atomic sites contribute to the molecule's overall interaction potential, aiding in

the interpretation of docking behaviour, conformational preferences, and structure–activity relationships. Thus, STM simulations serve as an important tool for probing the electronic landscape of mavacamten and enriching the theoretical understanding of its molecular interactions at the atomic scale.

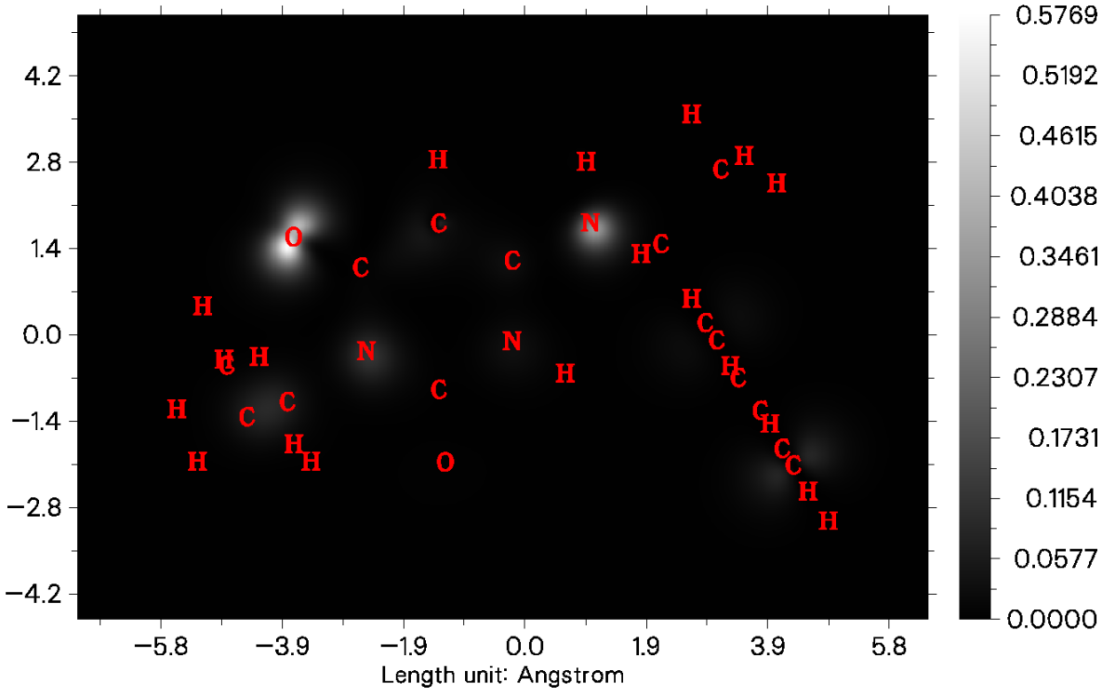

Figure 4: Simulated scanning tunneling microscope (STM) image of mavacamten

3.5.Shaded surface map with a projection of LOL investigation

The Localized Orbital Locator (LOL) (Eq. 2) is a quantitative function introduced by Schmider and Becke [18, 19] to identify regions of high electronic localization. It is defined through the dimensionless parameter $\tau(r)$, expressed as $g_0(r)/g(r)$, which depends entirely on the positive one-electron kinetic energy density, where $\varphi_i(r)$ denotes the Hartree–Fock or Kohn–Sham orbitals. A higher LOL value in a specific region indicates more confined electron motion, signifying strong localization.

$$\mathrm{LOL}(r) = \frac{\tau(r)}{1+\tau(r)} \qquad (2)$$

The shaded surface map depicting the LOL distribution for the title molecule, mavacamten, was generated and is presented in Figure 5. In this figure, blue shading on the carbon atoms corresponds to electron-depleted regions, whereas the red shading denotes areas of pronounced electron localization. The results clearly show that all carbon atoms exhibit regions of reduced electron density, while the aromatic hydrogen atoms display comparatively higher localized electron density. Furthermore, the localization pattern demonstrates that electrons tend to accumulate on the outer periphery of the aromatic rings, contributing to their stabilization.

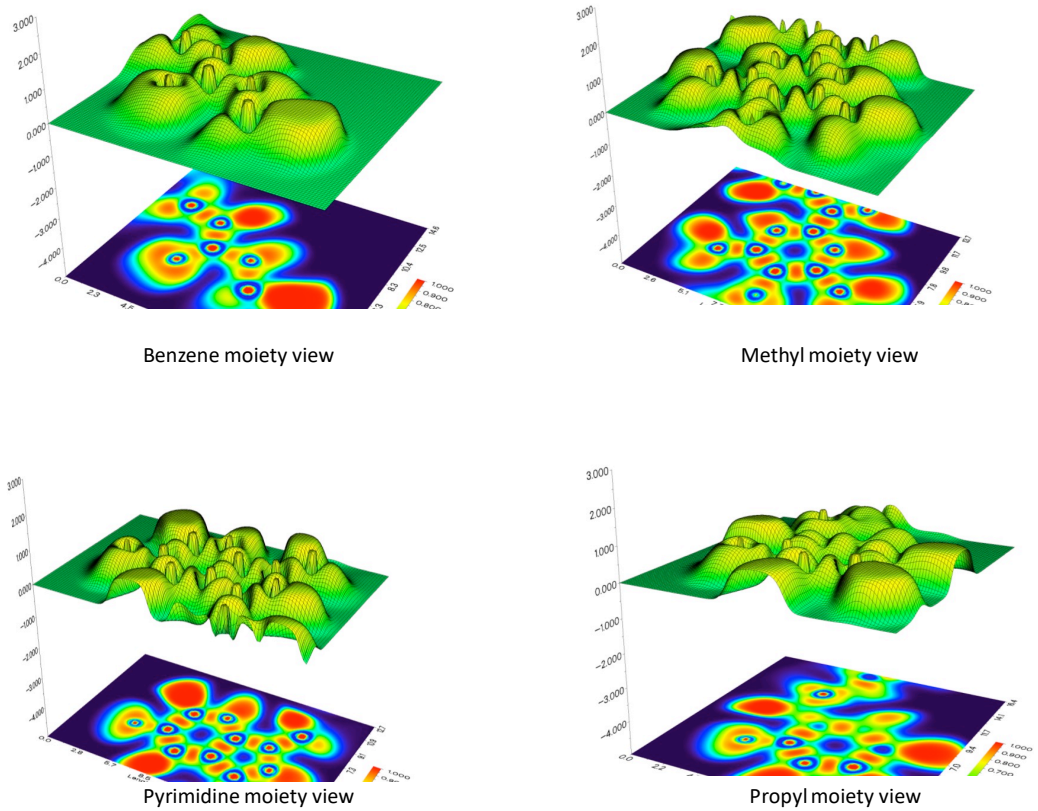

Figure 5: Shaded surface map with projection effect of electron localization function of mavacamten

3.6.Aromaticity

The structure of the molecule being studied includes a benzene ring. The aromaticity of the benzene ring of the title molecule is examined at the DFT/B3LYP/6-311G(d,p) level of theory. The Para Delocalization Index (PDI) [20], Bird Aromaticity [21], Aromatic Fluctuation Index (FLU) [22], Harmonic Oscillator Measure of Aromaticity (HOMA) [23], and PLR [24] data obtained using the Multiwfn 3.8 tool are displayed in Table 2. The FLU (equation 3), PDI (equation 4), HOMA (equation 5), BIRD aromaticity (equation 6), and PLR aromaticity (equation 7) are defined as follows:

$$\cdots = \frac{\cdot}{\cdot} \sum_{\cdot}^{\cdot} \left[\left(\frac{\cdot \cdot \cdot}{\cdot \cdot \cdot} \right) \left(\frac{\cdot \cdot \cdot \cdot \cdot - \cdot \cdot \cdot \cdot \cdot}{\cdot \cdot \cdot \cdot \cdot} \right) \right] \quad (3)$$

"Where n is equal to the number of atoms in the ring, δ_{ref} is the reference DI value, which is pre-calculated parameter. α is used to ensure the ratio of atomic valences is greater than one".

$$\cdots = \frac{\cdot \cdot \cdot + \cdot \cdot \cdot + \cdot \cdot \cdot}{\cdot} \quad (4)$$

$$\cdots = \cdot - \sum \frac{\cdot}{\cdot} \cdot \cdot \cdot \cdot - \cdot \cdot \quad (5)$$

"Where N is the total number of the atoms considered, j denotes the atom next to atom i, α and

R_{Ref} are pre-calculated constants given in original paper for each type of atomic pair".

$$I = \frac{V}{V_K} \text{ where } V = \frac{}{\bar{N}} \sqrt{\frac{\sum_i N_{i,j} - \bar{N}}{n}} \qquad N_{i,j} = \frac{a}{R_{i,j}} - b \quad (6)$$

"Where i cycles all of the bonds in the ring, j denotes the atom next to atom i. n is the total number of the bonds considered. N denotes Gordy bond order, $\bar{N}$ is the average value of the N values. $R_{i,j}$ is bond length. a and b are predefined parameters respectively for each type of bonds. V_K is pre-determined reference V".

$$PLR = A = B = \frac{\chi_{...} + \chi_{...} + \chi_{...}}{} \quad (7)$$

Figure 1 holds the information about the ring atom. The aromaticity of the mavacamten molecule was evaluated using multiple quantitative descriptors, including PDI, FLU, HOMA, BIRD, and PLR. The Para-Delocalization Index (PDI) value of 0.0995 indicates a moderate degree of electron delocalization within the aromatic ring, while the very low FLU value (0.0009) confirms a highly uniform electron distribution, characteristic of stable aromatic systems. The HOMA score of 0.9685 further supports this, as values approaching 1 denote near-ideal aromatic character. Additionally, the BIRD value of 98.0785 reflects strong bond equalization, reinforcing the high aromatic stabilization present in the ring. The PLR parameter (0.6066) also suggests substantial resonance-assisted delocalization. Together, these descriptors consistently demonstrate that mavacamten possesses a highly aromatic core with significant electronic delocalization and structural stability.

Table 2: The various aromaticity values determined for mavacamten

Aromaticity	Value
PDI	0.0995
FLU	0.0009
HOMA	0.9685
BIRD	98.0785
PLR	0.6066

3.7.Laplacian and Mayer bond analyses

Laplacian electron density is a real space function like ELF& LOL to reveal electronic structure for a molecule [25]. It is defined as:

$$\nabla^2 \rho(r) = \frac{\partial^2 \rho(r)}{\partial x^2} + \frac{\partial^2 \rho(r)}{\partial y^2} + \frac{\partial^2 \rho(r)}{\partial z^2} \quad (8)$$

Laplacian electron density is a real space function like ELF & LOL to reveal electronic structure for a molecule [25]. It is defined as It is determined with the help of Multiwfn 3.8 tool. The isosurface value set was -0.3; the image developed is given in Figure 6. The blue color represents holes, and the green color represents electrons. The Mayer bond order for this molecule is also calculated [26]. By the following relation, the selected data are given in Table 3.

$$I_{AB} = \Sigma_{a \epsilon A} \Sigma_{b \epsilon B} (PS)_{ab} (PS)_{ba} \quad (9)$$

Where p (density matrix) contains electron-occupation information for each pair of basis functions. **S (overlap matrix)** describes the overlap between basis functions (how much two

atomic orbitals overlap). a∈A: means **all basis functions that belong to atom A.** b∈B: means **all basis functions that belong to atom B.**

Table 3: Mayer bond order data for mavacamten

S. No.	Atoms	Mayer bond order values
1	8C-12C	1.9860
2	11C-12C	1.6269
3	16C-18C	1.7262
4	18C-20C	1.7497
5	19C-20C	1.6856
6	1O-11C	0.0533
7	5N-19C	0.0524
8	6C-10C	0.0540
9	9C-32H	0.0521
10	16C-37H	0.0530

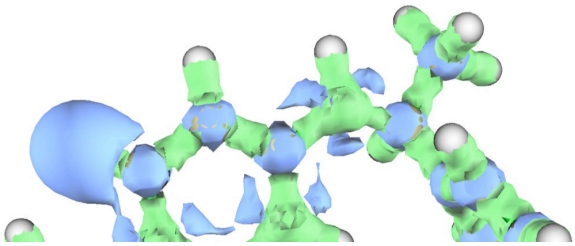

Figure 6: Laplacian electron density of mavacamten

The calculated Mayer bond orders provide valuable insight into the bonding characteristics and electron-sharing patterns within the molecule. The highest bond order is observed for the **8C–12C bond (1.9860)**, indicating a strong double-bond character consistent with significant π-electron delocalization. Similarly, the **11C–12C (1.6269), 16C–18C (1.7262), 18C–20C (1.7497)**, and **19C–20C (1.6856)** pairs exhibit moderately elevated bond orders, reflecting partial double-bond character and suggesting that these regions contribute to the conjugated framework or resonance-stabilized core of the structure. In contrast, the remaining interactions—**1O–11C, 5N–19C, 6C–10C, 9C–32H, and 16C–37H—**all show very low Mayer bond orders (~0.05), representing weak or negligible bonding interactions. These values typically arise from distant orbital overlap, hyperconjugative effects, or numerical remnants rather than true chemical bonds. Overall, the distribution of Mayer bond orders highlights a clear differentiation between strongly bonded carbon–carbon pairs involved in conjugation and very weak interactions that do not contribute meaningfully to the molecule's structural framework.

3.8.Core-Valence Bifurcation (CVB) Index

The CVB index is an additional descriptor used to evaluate the strength of intra- and intermolecular hydrogen bonding. For a hydrogen bond of the type A–H…B—where **A** represents the hydrogen-bond donor, **H** is the hydrogen atom, and **B** is the acceptor—the CVB index is determined using the expression:

CVB = ELF(C–V) – ELF(AH–B) **(10)**

In this equation, **ELF(C–V)** corresponds to the electron-localization-function value at the interface between the core and valence basins, while **ELF(AH–B)** refers to the ELF value at the point where the valence basins of the donor and acceptor begin to separate [27]. The conceptual illustration of the CVB index and its use in assessing hydrogen-bond strength is provided in Figure 7. **A negative CVB value** is associated with **strong hydrogen bonds,** indicating greater localization of electron density toward the acceptor in the A–H…B interaction**.** Conversely, a **positive CVB value** signifies **weaker interactions,** wherein electron density remains more localized near the donor atom. In general, **lower (more negative) CVB values correspond to stronger hydrogen-bond interactions [28].** For the molecule investigated in this study, the calculated ELF(C–V), ELF(AH–B), and corresponding CVB index values are reported in Table 4. The data in the table clearly show that mavacamten resulted in positive values, which shows weaker hydrogen bond interaction and that the electron density is more likely available in the donor atom surroundings.

Table 4: CVB index of mavacamten

$ELF_{(C\text{-}VD)}$	0.0935
$ELF_{(C\text{-}VA)}$	0.1317
$ELF_{(DH\text{-}A)}$	0.0637
CVB Index	0.0297

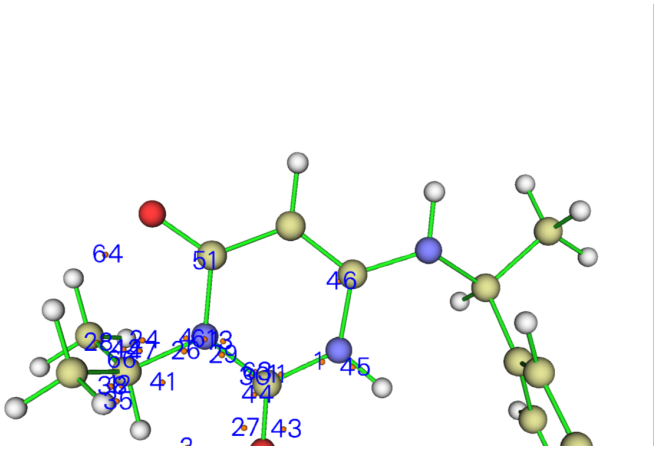

Figure 7: CVB index representation of mavacamten

3.9.Conclusion

The present DFT analysis offers an in-depth understanding of the structural and electronic features that shape the behavior of mavacamten at the molecular level. Mulliken charge distribution pinpointed chemically significant electron-rich and electron-poor centers, while NCI studies revealed the interplay of steric repulsion, dispersion forces, and weak hydrogen bonding that contribute to its conformational stability. The simulated STM images successfully mapped regions of high local density of states, supporting the observed reactivity trends around heteroatoms and aromatic segments. Multiple aromaticity descriptors collectively confirmed

that the benzene ring in mavacamten exhibits strong delocalization and remarkable structural stability. Laplacian electron density plots and Mayer bond order calculations further distinguished highly conjugated carbon–carbon bonds from negligible weak interactions scattered across the framework. Additionally, the positive CVB index values identified only weak hydrogen bonding tendencies, reinforcing the predominantly non-covalent nature of intramolecular stabilization. Overall, these computational insights not only clarify the electronic characteristics of mavacamten but also provide a valuable reference for designing derivatives, predicting interaction profiles, and extending theoretical studies on sarcomeric modulators.

4.Acknowledgements

The authors thank the authorities of St. John's College for supplying computers and software facilities.

5.Conflict of interest

The authors declare that, there is no conflict of interests regarding the publication of this article.

6.Funding

This research did not receive any specific grant from funding agencies in the public, commercial, or-not-for profit sectors.

7.References

1. Bello, J. and M.V. Pellegrini, *Mavacamten*, in *StatPearls [Internet]*. 2024, StatPearls Publishing.
2. Braunwald, E., et al. European Heart Journal vol. 44, pp. 4622-4633. (2023).
3. Zampieri, M., et al. Current cardiology reports vol. 23, pp. 79. (2021).
4. Heitner, S.B., et al. Annals of internal medicine vol. 170, pp. 741-748. (2019).
5. Edelberg, J.M., et al. American Journal of Cardiovascular Drugs vol. 22, pp. 497-510. (2022).
6. Parr, R.G. *Density functional theory of atoms and molecules*. in *Horizons of Quantum Chemistry: Proceedings of the Third International Congress of Quantum Chemistry Held at Kyoto, Japan, October 29-November 3, 1979*. 1989. Springer.
7. Frisch, M.e., et al., *Gaussian 16*. 2016, Gaussian, Inc. Wallingford, CT.
8. GaussView, V. Semichem Inc vol. pp. (2016).
9. O'boyle, N.M., A.L. Tenderholt, and K.M. Langner. Journal of computational chemistry vol. 29, pp. 839-845. (2008).
10. Lu, T. and F. Chen. Journal of computational chemistry vol. 33, pp. 580-592. (2012).
11. Celik, S. and E. Tanıs. Computational and Theoretical Chemistry vol. 1212, pp. 113709. (2022).
12. Contreras-García, J., et al. Computational and Theoretical Chemistry vol. 998, pp. 193-201. (2012).
13. Reed, A.E., L.A. Curtiss, and F. Weinhold. Chemical Reviews vol. 88, pp. 899-926. (1988).
14. Sagaama, A., et al. Journal of King Saud University-Science vol. 33, pp. 101606. (2021).
15. Jia, Z., et al. Theoretical Chemistry Accounts vol. 138, pp. 113. (2019).

16. Khan, S., et al. Journal of Molecular Liquids vol. 316, pp. 113860. (2020).
17. Donner, B., et al. American journal of physics vol. 73, pp. 690-700. (2005).
18. Schmider, H. and A. Becke. Journal of Molecular Structure: THEOCHEM vol. 527, pp. 51-61. (2000).
19. Bozorgmehr, M.R., J. Chamani, and G. Moslehi. Journal of Biomolecular Structure and Dynamics vol. 33, pp. 1669-1681. (2015).
20. Poater, J., et al. Chemical reviews vol. 105, pp. 3911-3947. (2005).
21. Bird, C. Tetrahedron vol. 41, pp. 1409-1414. (1985).
22. Matito i Gras, E., M. Duran i Portas, and M. Solà i Puig. vol. pp. (2005).
23. Krygowski, T.M. Journal of chemical information and computer sciences vol. 33, pp. 70-78. (1993).
24. Sablon, N., et al. Physical Chemistry Chemical Physics vol. 14, pp. 3960-3967. (2012).
25. Lu, T. and Q. Chen. Acta Physico-Chimica Sinica vol. 34, pp. 503-513. (2018).
26. Mayer, I. Chemical Physics Letters vol. 97, pp. 270-274. (1983).
27. Thomas, F. and R. Thomas. Journal of Molecular Liquids vol. 408, pp. 125404. (2024).
28. Khan, P., et al. Journal of Molecular Liquids vol. 393, pp. 123665. (2024).